Modulation of leukocyte homeostasis in atherosclerosis

Medina Rodriguez, I.A.

Modulation of Monocyte Migration and Macrophage Differentiation in Atherosclerosis

Janus Role of Hck and Fgr in Atherosclerosis Progression and Stability

Indira Medina, Oliver Soehnlein, Celine Cougoule, Rory R. Koenen, Yvonne Doering, Maike Drechsler, Beatriz Bermudez, Ine Wolfs, Veronica Herias, Ilze Bot, Saskia de Jager, Christian Weber, Jack Cleutjens, Theo J.C. van Berkel, Isabelle Maridonneau-Parini, Erik A.L. Biessen.
Submitted

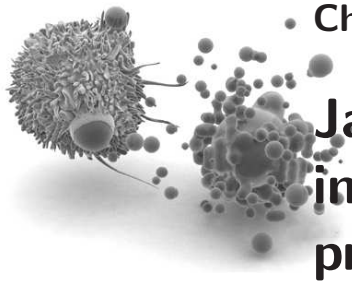

Chapter 2

Janus role of Hck and Fgr in atherosclerosis progression and stability

"With every day, and from both sides of my intelligence, the moral and the intellectual, I thus drew steadily nearer to the truth, by whose partial discovery I have been doomed to such a dreadful shipwreck: that man is not truly one, but truly two."
R. L. Stevenson, Dr. Jekyll and Mr. Hyde.

2.1 Abstract

Background: Leukocyte migration is critical for the infiltration of monocytes and the accumulation of macrophages in inflammation. Considering that Hck and Fgr are instrumental for this process, their involvement in macrophage accumulation in atherosclerosis and their influence in lesion formation and stability, was evaluated.

Methods and Results: Hematopoietic Hck/Fgr–deficient, LDLr$^{-/-}$ chimeras, obtained by bone marrow transplantation, had smaller lesions with fewer macrophages despite blood Ly6c^{hi} monocytosis. Hck/Fgr deficient monocytes and macrophages displayed impaired mesenchymal migration and disrupted adhesion and transmigration across endothelial monolayers *in-vitro* and established atherosclerotic plaques *in–vivo*, as assessed by intravital microscopy.

Reduced lesion size and macrophage infiltration, which is considered to induce lesion stability, were paradoxically contrasted by marked signs of lesion vulnerability such as reduced fibrosis and VSMC accumulation and expanded necrotic cores; implicating Hck and Fgr in lesion stability. Furthermore, SMC collagen deposition was reduced in SMC stimulated with conditioned medium from Hck/Fgr deficient macrophages. Gene expression analysis classical and alternative activated macrophages and human atherosclerotic lesions, indicated that Hck and Fgr are implicated in macrophage tissue repairing functions.

Conclusions: Combined hematopoietic deficiency of Hck and Fgr attenuated atherosclerotic plaque burden due to impaired endothelial adhesion and migration, but promoted plaque instability by causing monocyte subset imbalance and reduced macrophage tissue repairing functions.

2.2 Introduction

Inflammation and tissue repair are determinants of the clinical outcome of atherosclerosis, and are emerging now as two interrelated processes with many overlapping molecular mechanisms controlling monocyte infiltration and differentiation into macrophages, whose phenotype modulates the stability of lesions, by controlling the balance between matrix degradation and inflammation versus matrix deposition and wound healing [70].

Monocyte extravasation is an essential step for metabolic disease pathogenesis including atherosclerosis. The ability of monocytes to roll and adhere to the endothelium in response to chemokines is crucial for macrophage accumulation [6]. It relies on actin dependent morphological polarization, formation of filopodia and lamellipodia, binding of integrins to endothelial adhesion molecules, cytoskeletal reorganization [71] and signal transduction pathways ultimately leading to concerted loosening of adherent junctions on endothelial cells [72] and monocyte transmigration across endothelial, basement membrane and fibrous cap barriers, before their homing in expanding lesions and differentiation into macrophages that display either pro-inflammatory or tissue repairing phenotypes.

Hck and Fgr are two Src tyrosine kinases that display restricted co–expression and co–regulation in myeloid cells [73] where they induce LFA–1 integrin binding to endothelial ICAM to facilitate cell adhesion and migration upon PSGL–1 and CD44 interaction with endothelial E–selectin and P–selectin [74]. In addition, Hck and Fgr are a convergence point of signaling pathways initiated by a wide range of cell receptors implicated in the pathogenesis of atherosclerosis, including integrins, immune and growth factors, FcγR, adhesion and chemokine receptors.

These kinases exert their functions by activation of Rac/CDC42, Syk and Pyk [75] which are implicated in the accumulation and trapping of macrophages in atherosclerosis [76–79]. In addition, and as expected from signaling molecules downstream of multiple receptors, Hck and Fgr mediate a broad spectrum of cell processes, ranging from cell proliferation, survival and differentiation; to cytokine secretion, cytoskeleton dynamics, integrin dependent cell adhesion to the endothelium, and migration [75, 80–82].

In light of these data, Hck/Fgr–deficiency was hypothesized to lead to reduced accumulation of macrophages in atherosclerosis as consequence of reduced diapedesis and migration. The data here presented imply that Hck and Fgr control critical molecular processes that allow monocyte adhesion to the endothelium, mesenchymal migration, blood monocyte subset balance, macrophage accumulation and atherosclerotic lesion stability.

2.3 Materials and Methods

Animal Experiments: Bone marrow transplantation and perivascular collar placement experiments were approved by the local regulatory authorities of Leiden and Maastricht, and performed in accordance with the Dutch Government guidelines. For bone marrow transplantation experiments, female LDLr$^{-/-}$ recipient mice were obtained from the local animal breeding facility at the University of Leiden, Gorlaeus Laboratorium. Animals were exposed to a single dose of 9Gy total body ir-

radiation (0.19Gy/min, 200kV, 4mA) using an Andrex Smart 225 Rontgen Source (YXLON International, Copenhagen, Denmark) one day before reconstitution with bone marrow cells from wild–type C57Bl6/J mice obtained from Charles River Inc., or Hck/Fgr–deficient mice on C57Bl6/J background, kindly provided by Dr. Clifford Lowell (University of California, Department of Laboratory Medicine in San Francisco CA, USA) and bred at the local animal facility of CNRS/IPBS, Toulouse, France. Drinking water with antibiotics (83 mg/l ciprofloxacin and 67 mg/l Polymixin) and 5g/l sucrose was introduced one week before irradiation and supplied during the experiment. Mice were fed western type diet (0.25%cholesterol and 15% cacao butter; Special Diet Services, Witham, Essex, UK) during 13 weeks, starting eight weeks after bone marrow transplantation and ending at sacrifice.

The percentage of chimerism was used as a measure of bone marrow transplantation efficiency. It was determined as described previously [83], by quantification of the percentage of $LDLr^{+/+}$ present in genomic DNA obtained from peripheral blood of $LDLr^{+/+}Hck^{-/-}Fgr^{-/-}$ donor to $LDLr^{-/-}Hck^{+/+}Fgr^{+/+}$ recipient chimeras (PureLink Genomic DNA Purification Kit, Invitrogen). Samples were run in duplicate and CT values obtained from chimeras were used for interpolation of $LDLr^{+/+}$ DNA percentage by comparison to CT values obtained from a standard curve of a dilution series mix of 100% : 0% to 0% : 100% of $LDLr^{-/-}$:$LDLr^{+/+}$ mouse genomic DNA. CT values were calculated by Real–time PCR done with a Taqman IQ®SYBR Green Super Mix (BIO–RAD, Hercules, CA) in a MyiQ Icycler (Biorad) using LDLr specific primers (LDLr-forward: 5'-GCTGCAACTCATCCATATGCA-3' and LDLr-reverse: 5'-GGAGTTGTTGACCTCGACTCTAGAG-3'). A p50-specific primer set (P50-forward: 5'-AACCTGGGAATACTTCATGTGACTAA-3' and P50-reverse: 5'-GCACCAGAAGTCCAGGATTATAGC-3'); was used to standardize for the amount of imput DNA per sample.

Perivascular Collar Placement, Adoptive Fluorescent Cell Transfer and Intravital Microscopy: Perivascular collars were placed in female $LDLr^{-/-}$ (n=5), as described elsewhere [84]. Mice were fed western type diet containing 0.25% cholesterol and 15% cacao butter (W. Special Diet Services, Witham, Essex, UK) four weeks before collar placement and throughout the experiment. Mice were anesthetized twelve weeks after collar placement, once advanced plaques had formed, and a mixture of DAPI labeled Hck/Fgr double knockout (dKO) and DiI labeled wild type (WT) bone marrow derived macrophages (BMDM, $1X10^6$ cells each) was transferred by cardiac injection. Fifteen minutes after injection the left carotid was exposed for intravital microscopy recording during 1 minute, to quantify fluorescent labeled cell adhesion using an Olympus BX51 microscope equipped with a saline immersion 20X objective. Wounds were then sutured and animals allowed to recover from anesthesia and left one day until sacrifice to allow labeled cells to transmigrate to the plaques for analysis of *post mortem* cryosections by fluorescence microscopy.

Labeling of Circulatory Leukocytes and Intravital Microscopy Circulatory leukocyte adhesion *in–vivo* to the carotid artery was analyzed in WT versus Hck/Fgr dKO chimeras by intravital microscopy. For this, the right jugular vein was canulated with a catheter for antibody and dye injection. After exposure of the left carotid artery, antibodies (1μg) for CD11b (650NC, Ebiosciences), Ly6G (BioLegend), and Ly6C

(Ebiosciences) were administered to label various leukocyte subsets. Rhodamine 6G (100 l of a 0.1 solution) was injected to label all circulating leukocytes. Recordings were made 3 min after injection of each antibody. Intravital microscopy was performed using an Olympus BX51 microscope equipped with a Hamamatsu 9100–02 EMCCD camera and a 10x saline–immersion objective. For image acquisition and analysis Olympus Cell software was used.

Monocyte Labeling in LDLr$^{-/-}$ Hck/Fgr dKO Chimeras Chimeric mice generated by reconstitution of lethally irradiated LDLr$^{-/-}$ mice with bone marrow from Hck/Fgr dKO donors, received intravenous injections of Latex Beads (Polysciences) 18h after receiving chlodronate liposomes to label Ly6c^{hi} monocytes as described before [58]. Mice were sacrificed twenty four hours after labeling for excision of hearts and analysis.

Cholesterol and Triglyceride Levels: Blood samples were taken by tail bleeding one day before the introduction of western type diet, five weeks after introduction of WTD and at sacrifice. Total plasma, triglyceride and phospholipid contents were measured by an enzymatic–colorimetric assay (Roche Diagnostics, Almere, The Netherlands).

Plasma Cytokine Levels: The Luminex 100 Bio–Plex cytokine assay (Bio–Rad Laboratories, Inc; Hercules CA, USA) was used to determine cytokine expression in serum samples; cytokines investigated were: IL–1α, IL–1β, IL–2, IL–4, IL–5, IL–6, IL–10, IL–12(P40 and P70), IL–17, Eotaxin, Keratinocyte Chemoattractant (KC), Monocyte Chemoattractant protein–1 (MCP1), Monocyte inflammatory protein–1α (MIP1α) and Tumor Necrosis Factor–α (TNFα). Statistical analysis was performed for those cytokines that reached the limit of detection (IL–1β, IL–12, eotaxin, MCP1 and IL–1α).

Blood Cell Analysis and Flow Cytometry: Single cell suspensions of blood, bone marrow and peritoneal cells harvested at sacrifice were stained with fluorescent label conjugated antibodies after lysis of erythrocytes in ice cold NH_4Cl (8.4g/l) $NaHCO_3$ (1g/l) EDTA (37mg/l) during 3 minutes. Aortas were enzymatically digested with Liberase (Roche). Antibodies (eBioscience: B220 (25-0452-82, 1:150), CD11b (57-0112-82, 1:40), CD3e (45-0031-82, 1:50 or 11-0031-82, 1:300), CD19 (45-0193-82, 1:100 or 12-0193-83, 1:100), CD25 (17-0251-82, 1:300), MHCII(11-5322-82, 1:800), CD8a (48-0081-82, 1:300), FoxP3 (12-5775-82, 1:40), BD Pharmingen: Ly6G (551461, 1:100), CD11c (558079, 1:400), B220 (553089, 1:100), CD11b (552858, 1:300), CD4 (553052, 1:300), Miltenyi: Ly6c (130-093-134 or 130-093-136, 1:10) and Biolegend: F4/80 (123126, 1:25)) were used after Fc receptor blockage with CD16/32 blocking antibody (eBioscience 14-0161-85, 1:100). A FACSCanto II (BD Biosciences) flow cytometer coupled to the FACSdiva^{TM} software was used for acquisition and analysis of data. Whole blood samples were analyzed on a Sysmex blood cell analyzer (XT-2000i, Sysmex Europe GmbH, Norderstedt, Germany).

Cell Culture: Bone marrow derived from non adherent precursors and peritoneal macrophages were cultured in RPMI 1640 supplemented with mouse recombinant

M–CSF (20ng/ml, ImmunoTools, GmbH) or L929 conditioned medium (LCM, 15%) as previously described [85]. A clonal population of VSMC derived from C57Bl6 aortic explants was kindly provided by Dr. Eric van der Veer (Leiden University Medical Center. Leiden, The Netherlands) and cultured for less than 5 passages on 1% gelatin and 10μg/ml fibronecting coated wells with DMEM low glucose supplemented with 10% FCS, 2mM glutamine, 1% pyruvate, 100U/ml penicillin and 100μg/ml streptomycin. Human aortic endothelial cells, (HAoEC, PromoCell) were grown in endothelial growth medium MV (PromoCell). Jurkat (JS–10) lymphocytes were cultured in DMEM supplemented with 10% FBS, 2mM glutamine, 1% pyruvate, 100U/ml penicillin and 100μg/ml streptomycin.

Thioglycolate Induced Peritonitis: Cells were collected for analysis by FACS staining 1, 3 or 5 days (as indicated) after induction of peritonitis by intraperitoneal injection of a sterile solution of dehydrated Brewer's complete thioglycolate (TG) broth ($2-3\%$ w/v, Difco Laboratories, West Molesy, UK).

Phagocytosis Assays: Apoptosis was induced in cell tracker CMTMR (5μM, Molecular Probes) labeled Jurkat lymphocytes by incubation with staurosporine (1μM, Sigma) for 2h. The degree of apoptosis was $> 70\%$ as judged by AnnexinV and Propidium Iodide staining (BD biosciences) and flow cytometry. BMDM were incubated for 1h with LPS (10ng/ml) or complete medium, washed and incubated with labeled apoptotic cells (moi=20:1). Phagocytosis was analyzed on a FACSCanto flow cytometer with FACSDiva software (BD Biosciences), extracellularly bound particles were distinguished from internalized particles by excluding cell aggregates from singlets in FSC vs FSC and SSC plots. In separated experiments, BMDM were incubated with FITC–coupled zymosan particles (moi: $20:1$) opsonized by incubation with human IgG (13mg/ml in PBS, 20 min at 37^oC). Cells were washed, fixed with parafolmaldehyde (3.7%, Sigma), supplemented with 15mM sucrose, rinsed with PBS containing and stained with TRITC–conjugated antibodies. Yellow (FITC and TRITC positive) extracellular zymosan particles were distinguished from green FITC–positive internalized particles. Cells were counted by fluorescence microscopy to determine the percentage of cells that had ingested at least one particle.

Lipid Loading of BMDM: LDL was isolated from serum obtained from healthy volunteers using the density gradient ultracentrifugation method of Redgrave [86], oxidized with $CuSO_4$ (40μM, 37^oC, 24h) and dialyzed against PBS at 4^oC as previously described [87].

After incubation with 50μg/ml of LDL or oxLDL in 12–well plates, BMDM ($1x10^6$ cells per well) were detached from the culture surfaces, suspended in PBS and frozen at -20^oC for storage before further analysis. Cells were subsequently thawed and mechanically lysed by passing them through a 22 gauge needle attached to a 10 ml syringe. Cell lysates were resuspended to 0.25μg/μl of protein. Cholesterol acetate (20μg/ml in chloroform) was added as internal standard, to a total volume of 1200μl and samples centrifuged at 3000rpm, for isolation of the chloroform fraction. Lipid extracts were subjected to HP–TLC chromatography (Alltech/Applied Science) and analyzed for cholesterol content as described [88].

Macrophage Apoptosis and Proliferation: BMDM ($5x10^5$ cells/well) cultured on 0.2% gelatin coated 24–well plates, were serum–starved for 24h, incubated 48h in complete medium, harvested with EDTA (10mM) and stained with Propidium Iodide (50mg/ml) in PBS containing 2mM $MgCl_2$, 50units/ml DNAse free RNAse, 0.2% Triton X–100 (pH6.8). The same procedure was used for BMDM induced to undergo apoptosis by incubation with staurosporin (100nM) and/or LPS (10ng/ml) for 4h before harvesting. The proliferation index was calculated as the ratio of cells in the S, G2 and M phases of the cell cycle, relative to the total number of cells. The experiments were done in triplicate and the results averaged. Data acquisition and analysis was done by flow cytometry using a FACSCanto II (BD Biosciences) coupled to FACSdiva^{TM} software. No less than 10,000 cells were analyzed in each sample.

Macrophage Adhesion and Transmigration Across the Endothelium: Laminar flow assays were performed as described [89]. Briefly, endothelial HAoEC cells (PromoCell) were grown and pre–incubated with TNFα (10ng/ml) for at least 4h. Hck and Fgr mutant BMDM or WT controls were suspended at $5X10^5$ cells/ml in 1X Hank's buffer, 20mM Hepes, 0.5% HSA (Baxter) and 1mM calcium and magnesium after stimulation with IFNγ (100U/ml Peprotech) during 16 hours. For assessment of cell adhesion, macrophages were perfused over inflamed HAoEC monolayers during 2min at 0.1 ml/min and cells counted in 6 High Power Field (HPF, 100X magnification) pictures. Transmigration was recorded at a flow rate of 0.05 ml/min for 30min in 15sec intervals using a differential interference contrast (DIC) microscope.

Macrophage Morphology, Migration, Podosome Rosette Formation and Matrix Degradation: Transwell experiments: 100μl of Matrigel (BD Biosciences, batches from 8 to 10 mg/ml) or type I fibrillar collagen (2mg/ml Nutacon, Leimuiden, The Netherlands) were poured in transwells (8μm pores, BD Biosciences), polymerized at 37^{o}C for 30 minutes and 1 hour respectively, and rehydrated with RPMI 1640 to obtain dense matrices. $5x10^4$ BMDM (n=3) were seeded in the upper chamber on top of the matrices for assessment of macrophage mesenchymal and amoeboid migration respectively, as previously described [90, 91]. Gelatin–FITC matrix degradation and podosome structures were assessed as described [91]. Rosettes of podosomes were considered large or small when their diameter was respectively bigger or smaller than 20μm. When indicated a cocktail of protease inhibitors (PI, for composition see [91]) was added. Wound healing assay: BMDM monolayers on 0.2% gelatin coated 24 well plates ($0.5x10^6$ cells per well) were serum starved for 24h, scraped with a pipette tip, incubated 48h in complete medium and either photomicrographed for quantification of cell migration or collected for assessment of proliferation. Cell morphology and polarization: peritoneal macrophages (PEM) were judged to be elongated or rounded when displaying an Elongation Index (EI, defined as the ratio of cell length to breadth) respectively greater or lower than 2 or 1.2, 36h after collection and culture. Cells showing more than three filopodial extensions, were judged to possess filopodia [92].

Gelatin Zymography and β–Hexosaminidase Release: Zymography experiments were performed as previously described [91]. Briefly, BMDM ($1x10^6$ cells/well) were seeded overnight into 6–well fibronectin coated plates. Conditioned culture medium and cell lysates were subjected to 10% (w/v) SDS, 0.1mg/ml gelatin gel electrophore-

sis. For β–hexosaminidase release, BMDM (1x10^6 cells/well) were seeded overnight into 6–well plates, the assay was performed on cell extracts obtained in 1% Triton X100 and supernatants, as previously described [93].

Classic and Alternative Macrophage Polarization: Immune polarization of BMDM (5x10^5 cells/well in) BMDM were seeded at 5x10^5 cells/well in 24–well plates) was induced by plates and allowed to adhere overnight before immune polarization incubation either with 100U/ml IFNγ (Peprotech) or 20ng/ml IL–4 (Peprotech). RNA was isolated using a Nucleospin RNA II kit (Macherey Nagel, Duren, Germany). cDNA was obtained with the iSCript®cDNA synthesis kit (BIO–RAD, Hercules, CA). Real–time PCR was done with a Taqman IQ®SYBR Green Super Mix (BIO–RAD, Hercules, CA) in a MyiQ Icycler (Biorad). Cyclophilin was used as house keeping gene. Primer sequences are detailed in the Table 2.1. Samples were run in triplicate and the comparative C_t method was used for analysis. Ct values were defined as the cycle number at which the fluorescence signals were detected.

Gene	Forward Primer	Reverse Primer
INOS	5'CCTGGTACGGGCATTGCT3'	5'GCTCATGCGGCCTCCTTT3'
IL–18	5'CAGGCCTGACATCTTCTGCAA3'	5'TCTGACATGGCAGCCATTGT3'
IL–12p40	5'CGCAGCAAAGCAAGATGTGT3'	5'TGGAGACACCAGCAAAACGA3'
Arg	5'ATGGAAGAGACCTTCAGCTAC3'	5'GCTGTCTTCCCAAGAGTTGGG3'
IL–10	5'TCTTACTGACTGGCATGAGGATCA3'	5'GTCCGCAGCTCTAGGAGCAT3'
MR	5'GCAAATGGAGCCGTCTGTGC3'	5'CTCGTGGATCTCCGTGACAC3'
TGF-β	5'CCTGGGCACCATCCATGA3'	5'CCGCACACAGCAGTTCTTCTC3'
Cyclophilin	5'CAAATGCTGGACCAAACACAA3'	5'ACCTTCCCAAAGACCACAT3'

Table 2.1. *Primers Used for M1/M2 polarization in Hck/Fgr deficient BMDM.*

SMC Collagen Synthesis and Proliferation: Cell proliferation, extracellular collagen and non–collagenous protein deposition were assessed in VSMC cell layers by ELISA (Roche, BrdU colorimetric kit, Cat. No. 11647229001) and a quantitative collagen and protein micro–assay kit (Chondrex, Inc. Redmond, WA, USA), respectively; according to manufacturer's instructions.

Tissue Harvesting, FACS Analysis of Aortas, Immunohistochemistry and Plaque Morphometry: Mice were anesthetized and sacrificed. Animals were perfused with PBS followed by 4% formaldehyde before dissection of heart, aorta, common carotid arteries, spleen, thymus and liver. Aortas were enzymatically digested with Liberase TM (Roche) and single cell suspensions were stained for FACS analysis of macrophages and T lymphocytes. Samples of spleen, thymus, liver, lung and bone marrow were collected for analysis of gene expression and histology. Three samples per organ were obtained, one of which was snap–frozen in liquid nitrogen and stored at -80^{o}C. The other two samples were stored in 4% formaldehyde (4.5 times diluted Zinc Formal–Fix, Thermo Electron Corporation, Breda, The Netherlands) overnight, before being embedded, one in paraffin and the other in OCT compound (Tissue–Tek,

Sakura Finetek). Hearts were only embedded in OCT compound after fixation. Ten or five micrometer thick cryosections were obtained respectively from the aortic root or the carotids. Aortic root sections were stained using MOVAT's penthachrome procedure. Corresponding sections on separated slides were stained for α–naphthyl acetate esterase to detect monocytes and macrophages (Sigma–Aldrich); or with rat anti–Ly6G (1:200, Clone 1A8, BD Biosciences Pharmigen), Rabbit anti rat–biotin (Dako), ABC Alkaline Phosphatase (Vector Laboratories) and Vectastain Red (Vector Laboratories) for granulocytes. Picrosirius red was used for quantification of collagen. For analysis of Ly6c$^{+/+}$ monocyte infiltration, hearts of animals receiving beads were mounted with Dapi and used only for fluorescent microscopy. Cryosections from adoptive cell transfer, were analyzed by fluorescence microscopy. Sections were analyzed by two different blind observators, using the Leica Qwin Image Analysis Software, or ImageJ. All counterstains were done with hematoxylin.

Analysis of microarray Data: For micro–array analysis, total RNA was extracted using the Guanidine Thiocyanate (GTC),CsCl gradient method [94] and a NucleoSpin RNA II kit (Macherey Nagel, Duren, Germany). Comparison of gene expression was done for early (n=13) vs. advanced stable (n=16) lesions obtained after autopsy (Department of Pathology, University Hospital Maastricht, Maastricht, The Netherlands) or advanced stable (n=21) vs. advanced unstable (n=23) lesions obtained upon surgery (Department of Surgery, Maasland Hospital Sittard, Sittard, The Netherlands). RNA concentration was determined using a Nanodrop ND–1000 and RNA quality assessed using the RIN (RNA integration number) values obtained with an RNA 6000 Nano/Pico LabChip (Agilent 2100) Bioanalyzer. Samples where the RIN number was lower than 5.6 were excluded from the study. The mean RIN was 7.2$\pm$0.49. Samples from autopsy were individually hybridized to HGU133 2.0 Plus arrays (Affymetrix, Santa Clara, USA, California) and samples from surgery to Illumina Human Sentrix–8 V2.0 BeadChip (Illumina Inc., San Diego, USA, California). Plaques were staged by histological analysis of adjacent slides according to Virmani et al. [95]. Intimal thickening (IT), thick fibrous atheroma (TkfcA) and intraplaque hemorrhaged lesions (IPH) were characterized respectively as early, advanced stable and advanced unstable lesions, respectively. All human work was approved by the Ethics Committee of the University Hospital Maastricht. Written informed consent for participation in the study was obtained from all individuals. Microarray expression data of macrophage immune polarization was obtained at the Gene Expression Omnibus Web site (www.ncbi.nlm.nih.gov/geo) under accession number GSE18686 [96]. For analysis of advanced vs unstable and early vs advanced stable lesions, probe set normalization and summarization was performed using robust multi–array averaging RMA (RMA background subtraction, median polish summarization and quantiles normalization). Data normalization, summarization and statistical differences computed with permutation were assessed using respectively the R/Bioconductor packages Affy [97] and Maanova [98]. Probes mapping to single gene IDs were selected using the highest Hyndman's type 7 IQR [99] after non specific removal of low expression probes using MatLab's (Ver7.9) Bioinformatics Tool Box (Ver3.4). Genes with Benjamini Hochberg corrected false discovery rate and fold change (FC) $FC > 2$ were considered differentially expressed. K–means with permutation cluster analysis was performed using R/Maanova after cluster validation with SC^{2}ATmd in

MatLab [100]. Overrepresented biological categories within each cluster were identified using DAVID (Database for Annotation, Visualization and Integrated Discovery) [101] and InnateDB (Innate Immunity Interactions and Pathways) [102–104] databases. Cluster expansion was performed using Innatedb [102–104]. Transcription factor and transcription regulator analysis were performed using MRA-FET [105,106] in geWorkbench. The network used for MRA-FET was constructed using ARACNe with adaptive partitioning (P value treshold: 0.01) [107]. Transcription factors and transcription regulators in the whole GSE18686 dataset where found by overrepresentation analysis for gene ontologies GO:0006351 (transcription) and GO:0006355 (regulation of transcription) using InnateDB (Hypergeometric algorithm with Benjamini Hochberg correction) [102–104]. Pathway analysis was performed with KEGG system retrieved information using the SOAP/WSDL based web serviced from withing MatLab's bioinformatics toolbox. Venn diagrams were obtained withing Cytoscape (http://cytoscape.org) using a Diagram Generator application [108].

Statistical Analysis of Experimental Data: Non–parametric Mann–Whitney U test or t–test, were done as appropriate, using MatLab Software. Two sided P values < 0.05, were considered significant and denoted with one, two or three asterisks when lower than 0.05, 0.01 or 0.001, respectively. Data are presented as mean±SEM. Correlation analyses were performed by Spearman's rank correlation test. Correlations were compared with the Fischer R–to–Z transformation, and the F test was used to assess the significance of the difference between correlations. Multiple comparisons were analyzed by one–way ANOVA, followed by Bonferroni multi–comparison test.

2.4 Results

Deficiency in Hck and Fgr Leads to Reduced Atherosclerotic Lesions with Reduced Contents of Myelocyte Cells Despite Ly6c^{hi} Monocytosis: Atherosclerosis prone chimeric mice were generated by reconstitution of lethally irradiated LDLr$^{-/-}$ recipient animals with Hck$^{-/-}$Fgr$^{-/-}$ double Knock–Out (dKO) or Wild Type (WT) bone marrow cells, to establish the role of leukocyte Hck/Fgr–deficiency in atherosclerosis onset and progression. An average of 95.9% of white blood cells was of donor origin, indicating successful engraftment. Hck/Fgr deletion did not lead to any alteration in total body weight along the experiment nor did it affect total plasma cholesterol levels before (199.4 mg/dl vs. 150.8 mg/dl for WT controls), and after (1616.1 mg/dl vs. 1488.9 mg/dl, for WT controls) WTD introduction. Plasma cytokine levels of IL–1β, IL–12, Eotaxin, MCP1, and IL–1α, measured at sacrifice, were not influenced by Hck/Fgr–deficiency (Appendix A. Fig. A.1).

Chimeric mice transplanted with Hck/Fgr dKO bone marrow exhibited 37% ($P \leq 0.01$) reduction in atherosclerotic lesion size (Fig. 2.1A), coupled with 34% ($P \leq 0.001$) and 61% ($P \leq 0.05$) reduction in intimal macrophage and adventitial neutrophil contents, respectively (Fig 2.1B-C). FACS analysis of atherosclerotic aortas confirmed reduction in macrophage accumulation (Appendix A. Fig. A.2A) and further indicated that deficiency in Hck/Fgr had no effect in lymphocyte accumulation in atherosclerotic lesions (Appendix A. Fig. A.2B). A similar reduction was observed in the peritoneal cavity of dKO chimeras 120 hours after induction of peritonitis with thioglycolate (TG) (Appendix A. Fig. A.3A-C) where no differences in

the activation of macrophages were observed, as assessed by the expression of CD86, CD40 and MHCII (Appendix A. Fig. A.3D); suggesting that Hck/Fgr–deficiency did not perturb the activation potential of atherosclerotic lesion macrophages. Correlation analysis indicated delayed development of atherosclerotic lesions, as intimal macrophage area correlated well to plaque size (Appendix A. Fig. A.4A) both in WT controls (Spearman's correlation coefficient: $R = 0.9636$, $P \prec 0.0001$) and mutant chimeras ($R = 0.9833$, $P \prec 0.0001$). Correlation coefficients were not significantly different between groups ($P = 0.5$). Adventitial neutrophil contents did not correlate to lesion size, neither in dKO chimeras nor in WT controls (Appendix A. Fig. A.4B).

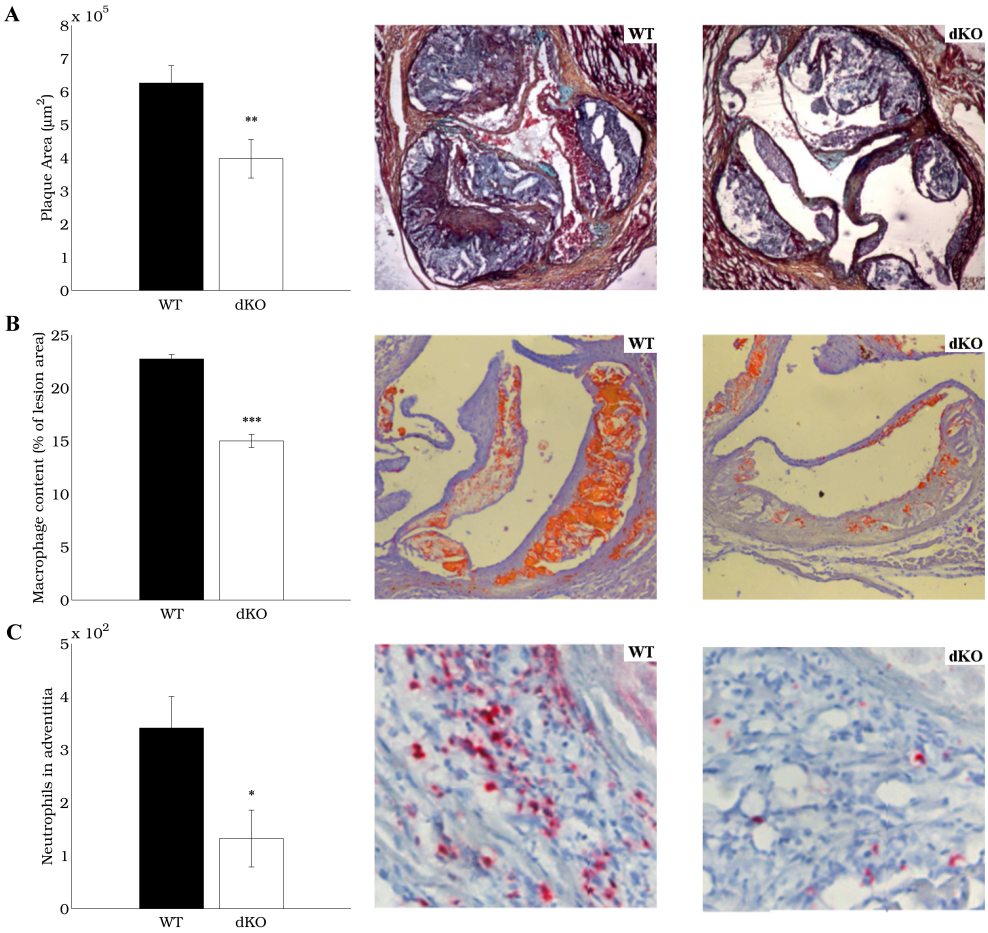

Figure. 2.1. *Reduced lesion size and myeloid cell accumulation in dKO Hck/Fgr chimeras. Hck/Fgr–deficiency caused 37% reduction in atherosclerotic lesion size (n=13, 10 sections per experimental unit) in aortic roots of WTD fed LDLr$^{-/-}$ mice (A). Intimal macrophages (B) and adventitial neutrophils (C), were reduced by 34% and 61%, respectively. Middle and right panels in A-C display representative slides of plaque size, macrophage and neutrophil stainings, respectively. ($*P \leq 0.05$, $**P \leq 0.01$, $***P \leq 0.001$).*

Leukocyte subsets levels were quantified in blood, bone marrow and spleen, to assess the effect of Hck/Fgr–deficiency and determine whether the reduced contents of macrophages and neutrophils observed in atherosclerotic lesions was caused by reduced availability in the circulation or impaired hematopoiesis or extravasation of myelocyte precursors.

The absolute and relative levels of circulatory, bone marrow and spleen white blood cells, T (cytotoxic, helper and Tregs) and B lymphocytes, as well as of spleen dendritic cells (DC, resident and plasmacytoid), were not disturbed in chimeric mice fed WTD (data not shown). Similarly, equivalent bone marrow myelocyte cell composition (Appendix A. Fig. A.5A) and monocyte subset levels (Appendix A. Fig. A.5B) were observed. In addition, Hck/Fgr deficiency did not influence the expression of Ly6c in blood monocyte subsets (Appendix A. Fig. A.5C-D) nor the absolute and relative levels of circulatory myelocytes (Appendix A. Fig. A.5E-F). However, a significant increase in Ly6c^{hi} monocytes (+23%, $P \prec 0.01$), caused marked blood Ly6c^{hi} monocytosis (Appendix A. Fig. A.5G), suggesting that less macrophages extravasated into atherosclerotic lesions, despite higher availability of blood Ly6c^{hi} monocytes.

Lack of Hck/Fgr Leads to Reduced Monocyte Adhesion to the Endothelium and Recruitment Into Atherosclerotic Lesions Explaining the cause of reduced accumulation of dKO macrophages in atherosclerotic lesions induced in dKO chimeras, intravital microscopy of *in–vivo* labeled cells demonstrated reduced leukocyte adhesion to atherosclerotic lesions (Fig. 2.2A-C). In fact, reduced counts of CD11b^{+} myelocytes (Fig. 2.2A), as well as Ly6G^{+} granulocytes (Fig. 2.2B) and Ly6c^{hi} monocytes (Fig. 2.2B) were observed on carotid lesions of dKO–LDLr$^{-/-}$ chimeric mice, compared to WT–LDLr$^{-/-}$ controls. In agreement with these results, reduced levels of newly recruited Ly6c^{hi} monocytes were observed, twenty four hours after labeling with fluorescent beads (Fig. 2.3A-C).

Similarly, adoptively transferred fluorescent labeled dKO BMDM displayed profoundly reduced adhesion (-67%, $P \leq 0.001$) and almost ablated transmigration (-88%; $P \leq 0.001$) to preexisting atherosclerotic lesions induced in WTD fed LDLr$^{-/-}$ mice by perivascular collars (Fig. 2.4A-D). Matching these results *in–vivo*, dKO BMDM perfused through a monolayer of inflamed endothelium *in-vitro* displayed reduced adhesion (Fig. 2.4 E-F). Once adhered, the percentage of cells that transmigrated across the endothelium *in-vitro* was not influenced by Hck/Fgr–deficiency (Fig. 2.4G), implying that transendothelial macrophage migration was reduced indirectly by prior impairment of the adhesion mechanism.

In-vitro, dKO BMDM displayed reduced cell densities on the scraped area in wound healing assays (-94%, $P \leq 0.001$; Fig. 2.5A), despite that proliferation rates (Appendix A. Fig. A.6A) and seeded cell densities were similar in both genotypes, indicating impaired two dimensional migration. In addition, dKO peritoneal macrophages (PEM) presented altered morphology *in-vitro* characterized by lack of elongation and morphological polarization, and reduced formation of filopodium and lamellipodium (Fig. 2.5B-F); suggestive of dysfunctional actin network polymerization.

Taken together these results indicate impaired monocyte adhesion on the endothelium and disrupted diapedesis, as contributing factors to the reduced accumulation of macrophages observed in atherosclerotic dKO chimeras.

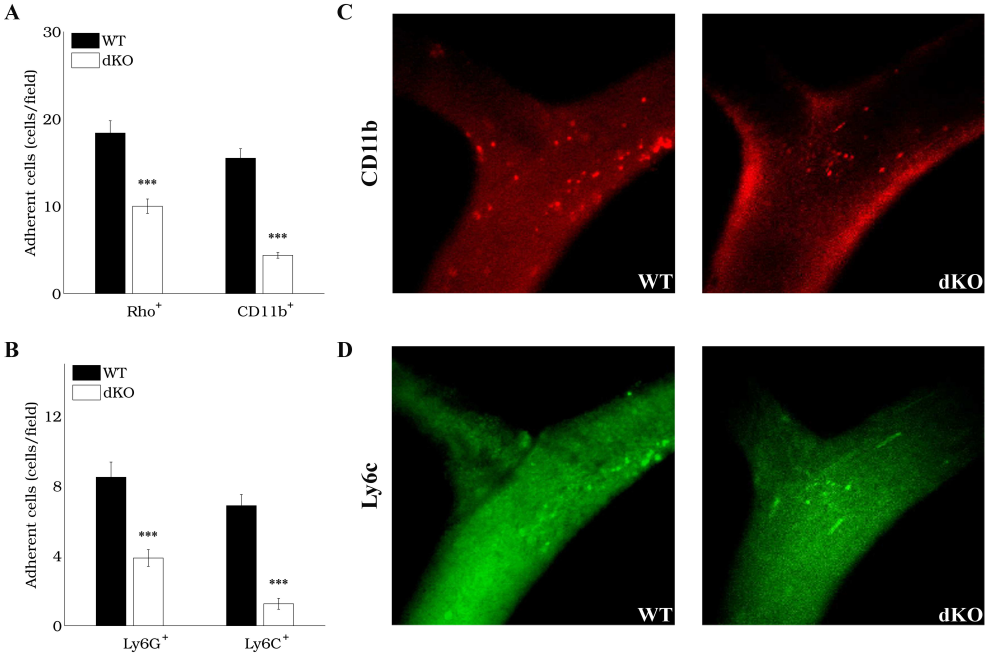

Figure. 2.2. *Impaired adhesion to the endothelium and transmigration of Hck/Fgr–deficient circulatory leukocytes. Circulatory leukocyte adhesion to the carotid artery was analyzed in WT versus Hck/Fgr dKO chimeras by intravital microscopy. For this, the right jugular vein was canulated with a catheter for dye and antibody injection after exposure of the left carotid artery. Intra–vital microscopy recordings were made three minutes after injection of Rhodamine or antibodies for CD11b, Ly6G and Ly6C were administered. A-D. Reduced adhesion of Rhodamine$^+$ fluorescent blood leukocytes (A) labeled in in–vivo were observed in dKO–LDLr$^{-/-}$ chimeras, compared to WT–LDLr$^{-/-}$ control mice. Similar reductions were observed in circulatory CD11b$^+$ myelocytes (A) as well as Ly6G$^+$ neutrophils and Ly6c$^+$ monocytes (B). C-D. Representative pictures of intravital microscopy corresponding to CD11b$^+$ labeled myelocytes and Ly6c$^+$ circulatory monocytes (D). ***P=0.001.*

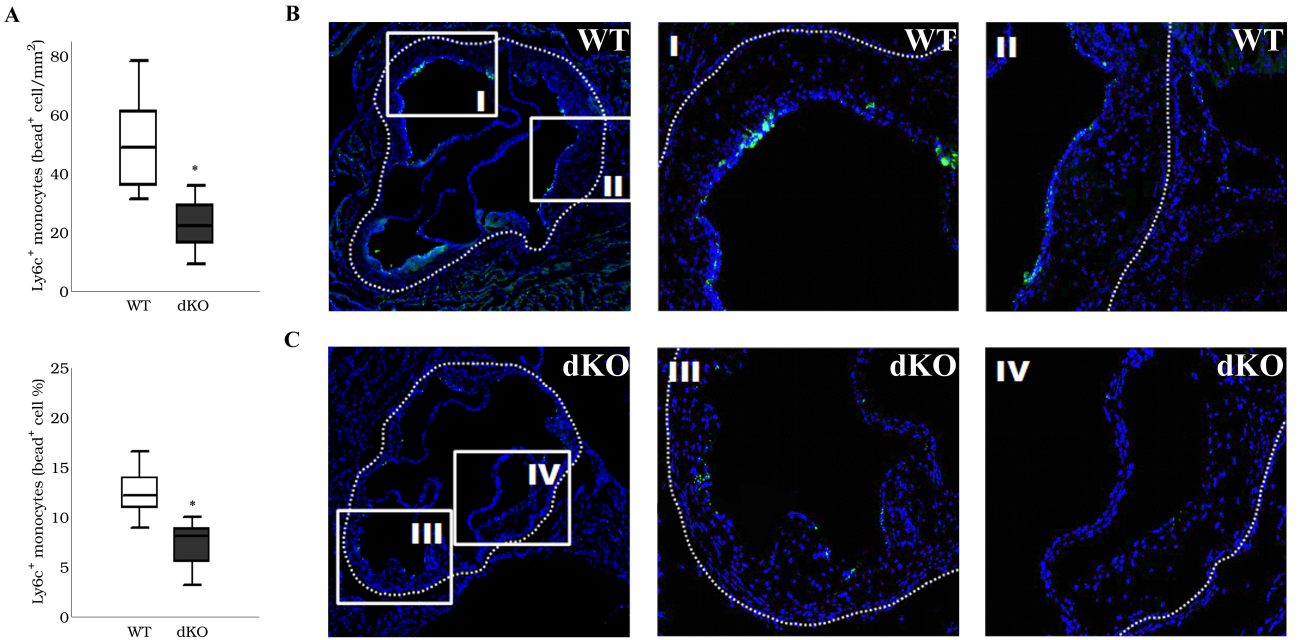

Figure. 2.3. *Hck/Fgr deficiency causes reduced accumulation of newly recruited Ly6c^{+} monocytes in atherosclerotic lesions. A-C. Chimeric mice were generated by reconstitution of lethally irradiated LDLr$^{-/-}$ mice with bone marrow from Hck/Fgr dKO donors. These animals received intravenous injections of Latex Beads 18h after receiving chlodronate liposomes to label Ly6c^{hi} monocytes [58]. Mice were sacrificed twenty four hours after labeling for excision of hearts and analysis by fluorescent microscopy of aortic root sections. A. Reduced accumulation of newly recruited monocytes was observed in dKO chimeras, compared to WT controls. B-C. Representative pictures of sections used for quantification of bead labeled monocytes (green). DAPI was used for staining of cell nuclei.(Scale bars in B-C, left panels: 500µm. Central and right panels: 100µm. Pictures in central and right panels correspond to zoom in micro–photographies of inserts in left panels)*

Hck/Fgr–Deficient Macrophages Display Reduced Three–Dimensional Migration The three–dimensional migration capacity of dKO macrophages was next assessed, taking into account that particularly at late stages of lesion development, extravasated cells must pass through collagen and VSMC rich fibrous caps. Macrophages employ mesenchymal and amoeboid migration mechanisms to perform three dimensional infiltration [90] either by protease dependent degradation of dense Extracellular Matrices (ECM) or by squeezing and deforming their cell body across similar sized pores, respectively.

In-vitro, dKO macrophages displayed unimpaired amoeboid migration across type I fibrillar collagen (Fig. 2.6A), which contrasted with their markedly inhibited mesenchymal migration through dense Matrigel (Fig. 2.6B). Furthermore, the addition of Proteinase Inhibitors (PI) inhibited the mesenchymal migration through matrigel in WT BMDM to levels observed in untreated mutant cells. PI were however unable to further impair the migration capacity of mutant BMDM (Fig. 2.6B) suggesting that Hck/Fgr–deficiency caused reduced mesenchymal migration either by downregulating the expression or disrupting the release of proteases. However, dKO BMDM displayed no abnormality in lysosomal secretion of β–hexosaminidase (Fig. 2.6C), MMP2 and MMP9 (Fig. 2.6D), excluding that vesicular secretion defects had underlaid the observed impairment of macrophage migration.

During mesenchymal migration, protease delivery is thought to take place at podosomes [90]. The formation of podosomes and their organization as rosettes was therefore assessed. As previously shown, podosome rosettes are structures formed upon Hck activation in Macrophages [91,93], used for focal release of proteases at sites of cell penetration, to allow cell passage without distal ECM degradation [109]. As expected, WT cells formed large podosome rosettes; dKO cells in contrast, formed less and smaller podosome rosettes (Fig. 2.6E-F). Moreover, dKO macrophage rosettes had reduced ECM degradation capacity as assessed by FITC gelatin degradation (-44%, $P \leq 0.001$. Fig. 2.6G-H).

Taken together these results indicate that Hck/Fgr gene deletion causes reduced mesenchymal migration by impairing the formation of podosome rosettes leading to reduced pericellular degradation of the ECM, which likely contributed to the reduced accumulation of macrophages observed in atherosclerosis, by impairing their migration through lesion fibrous caps.

Hck/Fgr–Deficiency Promotes a Potentially Vulnerable Plaque Phenotype Despite their reduced size and macrophage contents, plaques from Hck/Fgr dKO chimeras unexpectedly exhibited a vulnerable plaque phenotype, characterized by necrotic core expansion (+68%; $P \leq 0.01$), and significant reductions in minimal fibrous cap thickness (-53%, $P \leq 0.001$) SMC (-75%, $P \leq< 0.001$) and collagen contents (-82%, $P \leq< 0.001$) (Fig. 2.7A-F). Statistical analysis revealed that except for necrotic core size, these variables did not correlate with lesion size (Appendix A. Fig. A.4C-F).

The possibility that dKO macrophages displayed increased apoptosis and/or reduced phagocytosis was therefore evaluated, as they correlate with necrotic core expansion and lesion vulnerability. In agreement with this, increased susceptibility to apoptosis induction was observed in dKO macrophages, compared to WT controls (Appendix A. Fig. A.6B). However, Hck/Fgr–deficient BMDM exposed normal phagocytosis of beads, apoptotic cells and opsonized particles, and uptake of modified

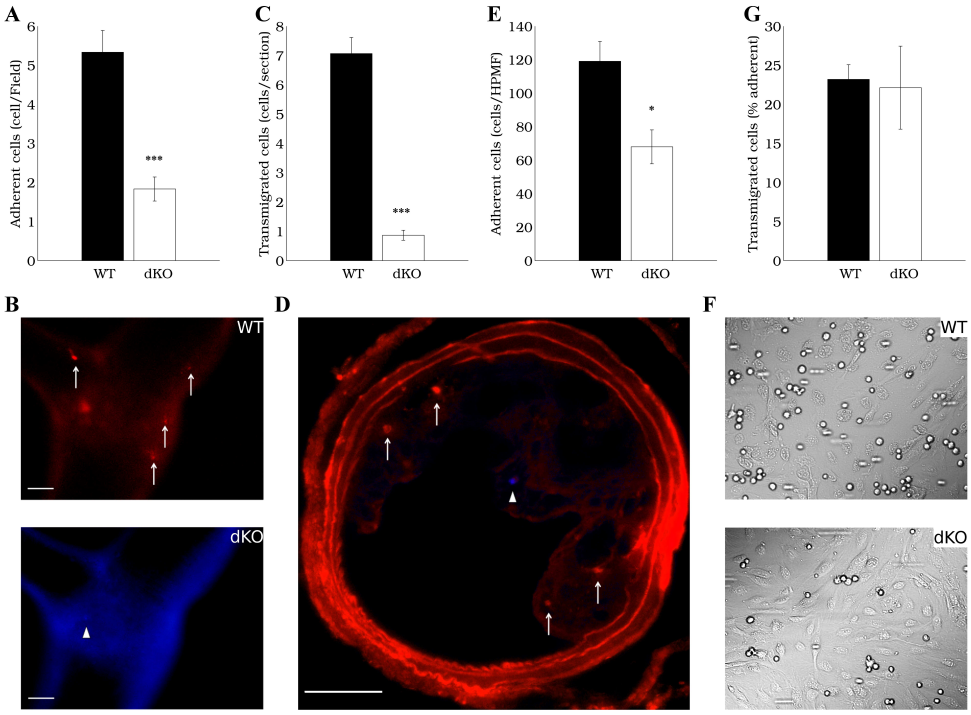

Figure. 2.4. *Impaired adhesion to the endothelium and transmigration of Hck/Fgr–deficient macrophages. Fluorescent labeled dKO macrophages adoptively transferred to LDLr$^{-/-}$ mice displayed reduced adhesion to (A-B) and diapedesis into (C-D) preexisting atherosclerotic lesions induced by perivascular collar placement (n=6). Representative pictures of intravital microscopy (B) and fluorescence microscopy (D) correspond to experiments depicted in A and C, respectively. DAPI labeled Hck/Fgr dKO (arrowheads, blue) and DiI labeled WT (arrows, red) BMDM, are shown to adhere to the endothelium in–vivo (B) and home to the subendothelial space (D, Postmortem section) 15 min (B) and 1 day (D) after cell co–transfer (10^6 BMDM/genotype/mouse) into atherosclerotic LDLr$^{-/-}$ mice (Scale bar: 100μm). Adhesion (E-F) but not transmigration (G) across monolayers of inflamed endothelium (in-vitro) is reduced in dKO BMDM (n=3, 6 High Power Microscopic Field (HPMF) quantifications per sample). (F. Representative differential Interference Contrast Microscopy HPMF pictures of BMDM adherent to inflamed endothelium in-vitro). (*P=0.05, ***P=0.001).*

cholesterol, *in-vitro* (Appendix A. Fig. A.6C-F).

In addition, incubation of VSMC layers with conditioned medium (CM) from unstimulated Hck/Fgr dKO BMDM did not influence their proliferation (Fig. 2.8A), but reduced their deposition of extracellular collagen and non–collagenous proteins akin to conditioned medium from LPS–stimulated WT macrophages and starvation medium (SM) (Fig. 2.8B-C) indicating that Hck/Fgr–deficiency causes skewed macrophage differentiation with reduced tissue repairing capacity and–or increased ability

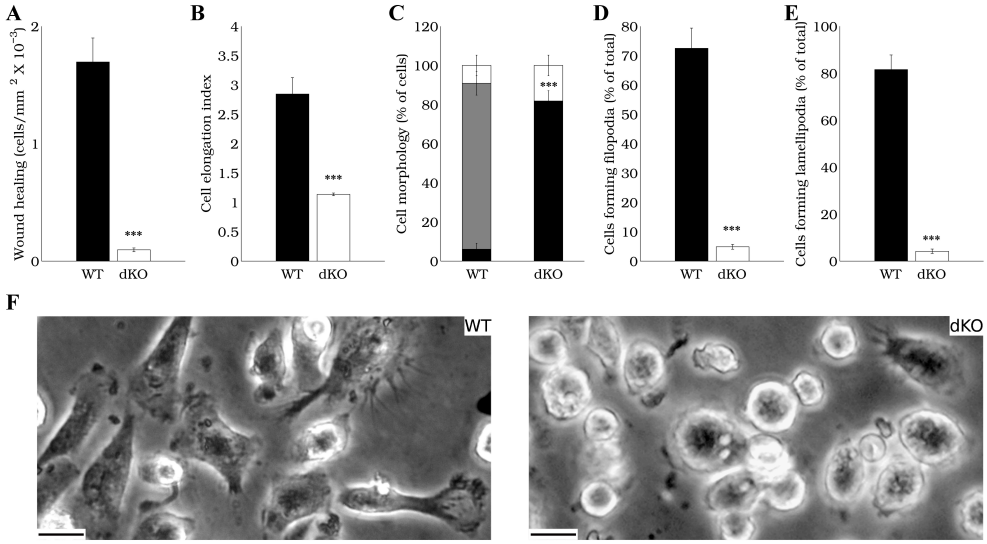

Figure. 2.5. *Hck/Fgr dKO macrophages display impaired two dimensional directional migration and aberrant morphology. A. dKO macrophages display* 94% *reduced two dimensional migration and wound healing capacity in-vitro (n=3, 5 area quantifications per replicate). B-C. Morphology of peritoneal macrophages (PEM) cultured for 36h (n=5, 100 cells per replicate). B. Mean elongation index (EI), defined as the ratio of cell length to cell breadth). C. Percentage of rounded ($EI \leq 1.2$ black bar segments), elongated ($EI \geq 2$,grey bar segments) and partially elongated cells ($1.2 \prec EI \prec 2$, white bar segments) as judged by the elongation index (EI). D-E. Percentage of PEM cultured for 16 hours, forming filopodia (D) and Lamellipodia (E) (n=5, 100 cells per replicate). F. Representative pictures depicting rounded cell morphology in dKO cells compared to WT PEM (Scale bar:* $10\mu m$. $***P \leq 0.001$*).*

to degrade the extracellular matrix.

The participation of Hck and/or Fgr in tissue repairing gene networks was assessed by transcriptome analysis of differentially expressed genes from human macrophages stimulated with TNFα, IL–4, IL–17, LPS, IFNγ or LPS+IFNγ (GSE18686, [96]). K–means cluster analysis of gene expression data revealed five gene clusters of which clusters III and IV (C-III and C-IV) contained respectively FGR and HCK (Fig. 2.9A).

Principal component analysis (PCA) indicated that C-I, C-II and C-III on one hand, and C-IV along with C-V, on the other, contained genes with upregulated expression in response to IL–4 and LPS–IFNγ, respectively (Fig. 2.9B, see also Appendix A. Fig. A.7 and A.8); suggesting that HCK and FGR participate in different molecular networks that determine the polarization phenotype of macrophages, in agreement with their differences in structure and classification withing the Src family of tyrosine kinases [110].

Consistently, HCK and FGR were higher than two fold regulated in response to IFNγ and IL–4 respectively (Fig. 2.9C). Transcription factor analysis predicted

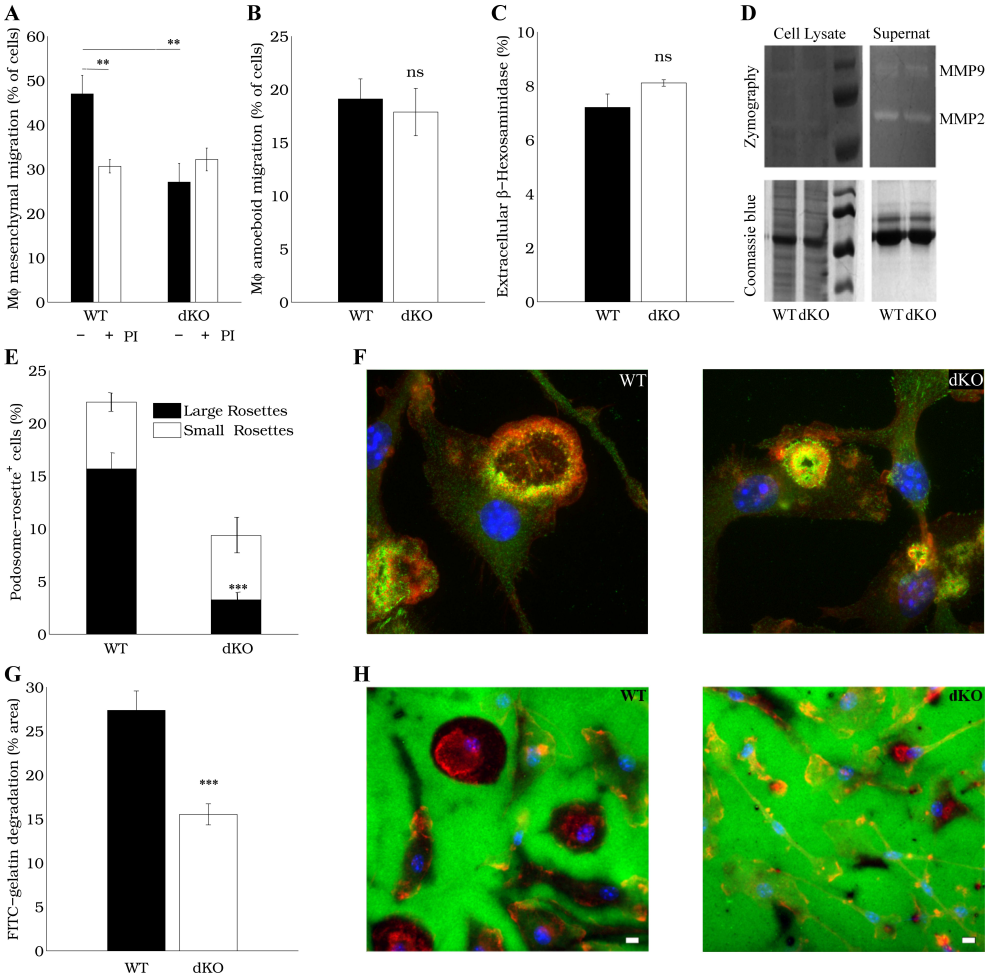

Figure. 2.6. *Assessment of three–dimensional migration. Hck/Fgr–deficient BMDM displayed normal amoeboid (n=3) (A) but reduced mesenchymal migration (n=3) across Matrigel transwells where proteinase inhibitors (PI) inhibited WT but not dKO BMDM migration (n=2). C. β–hexosaminidase was released at similar levels in WT and dKO BMDM (n=3). D. Metalloproteinases MMP–2 and MMP–9 content and secretion, assessed gelatin zymography, is unaffected in dKO BMDM. E. dKO BMDM form less and smaller podosome rosettes than WT controls (n=5). F. Representative pictures illustrating reduced podosome rosette size in dKO BMDM, 100X magnification. G. FITC–gelatin degradation is reduced in dKO BMDM (n=9). H. Representative pictures of BMDM showing fewer, smaller and paler gelatin proteolysis areas (in dark) colocalizing with podosome rosettes in dKO BMDM compared to WT controls. (Blue for cell nuclei, red for F–actin in F and H. Green for Vinculin in F, and FITC–gelatin in H). ($** P \leq 0.01$, $*** P \leq 0.001$).*

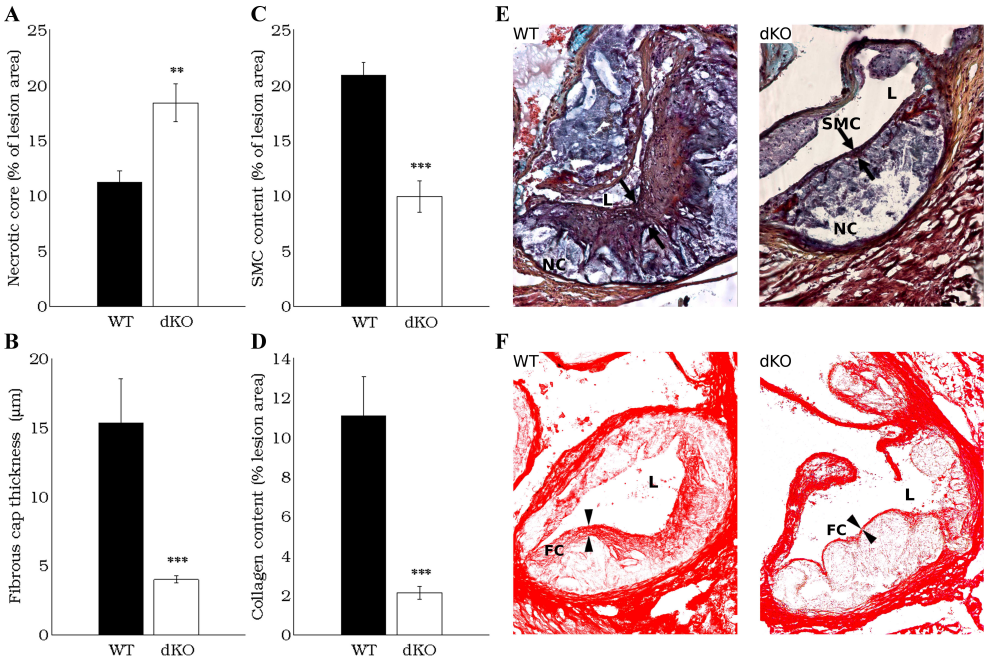

Figure. 2.7. *Atherosclerotic lesion composition in Hck/Fgr dKO atherosclerotic chimeras. Atherosclerotic lesions from Hck/Fgr dKO chimeras display features of plaque vulnerability characterized by bigger necrotic cores (+68%)(A) thinner fibrous caps (-53%) (B) and reduced SMC (-75%) (C) and collagen (-82%) contents (D) (n=13, 6 sections per experimental unit). E-F. Representative pictures denoting lumen size (L) necrotic core (NC) expansion, minimal fibrous cap (FC) thinning and reduced VSMC (arrows delimited red–purple areas in Movat's staining E) and collagen areas (Picrosirius Red staining, F) in dKO chimeras.* ($**P \leq 0.01$, $***P \leq 0.001$).

that positive regulators of gene expression associated with alternative activation of macrophages (HIF2A–EPAS1, IRF4, KLF2, KLF4, MAF, MYC, PPARγ, STAT3 and STAT6) regulated the expression of genes belonging to C-I, C-II and C-III (Fig. 2.9D and 2.10). In particular the expression of FGR was predicted to be positively regulated by STAT3, PPARG and KLF2 ($Pval \prec 0.0001$).

Similarly, transcription factors linked to classical activation of macrophages (HIF1α, IKBKG, JUND, NFKB, SOCS3, STAT1, STAT2,STAT5) acted as positive regulators of gene expression for clusters C-IV and C-V (Fig. 2.9E and 2.11). IKBKG and NFKB1 were found to be positive regulators of HCK expression.

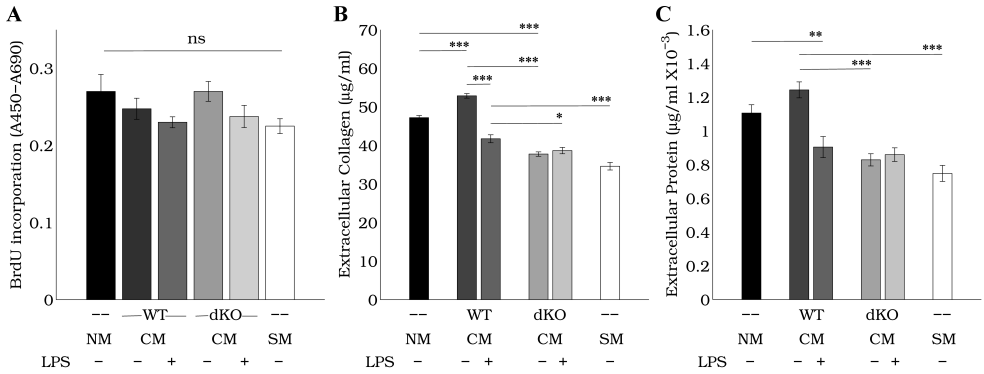

Figure. 2.8. *Conditioned medium from Hck/Fgr dKO BMDM attenuates VSMC collagen deposition. Despite similar proliferation rates (A), VSMC cultured during 48 hours with starvation medium (SM) and conditioned medium (CM) from dKO BMDM or WT LPS activated BMDM, displayed reduced extracellular deposition of collagen (B) and non collagenous proteins (C), compared to VSMC cultured in CM from WT BMDM. (n=4,* $*P \leq 0.05$, $**P \leq 0.01$, $***P \leq 0.001$*).*

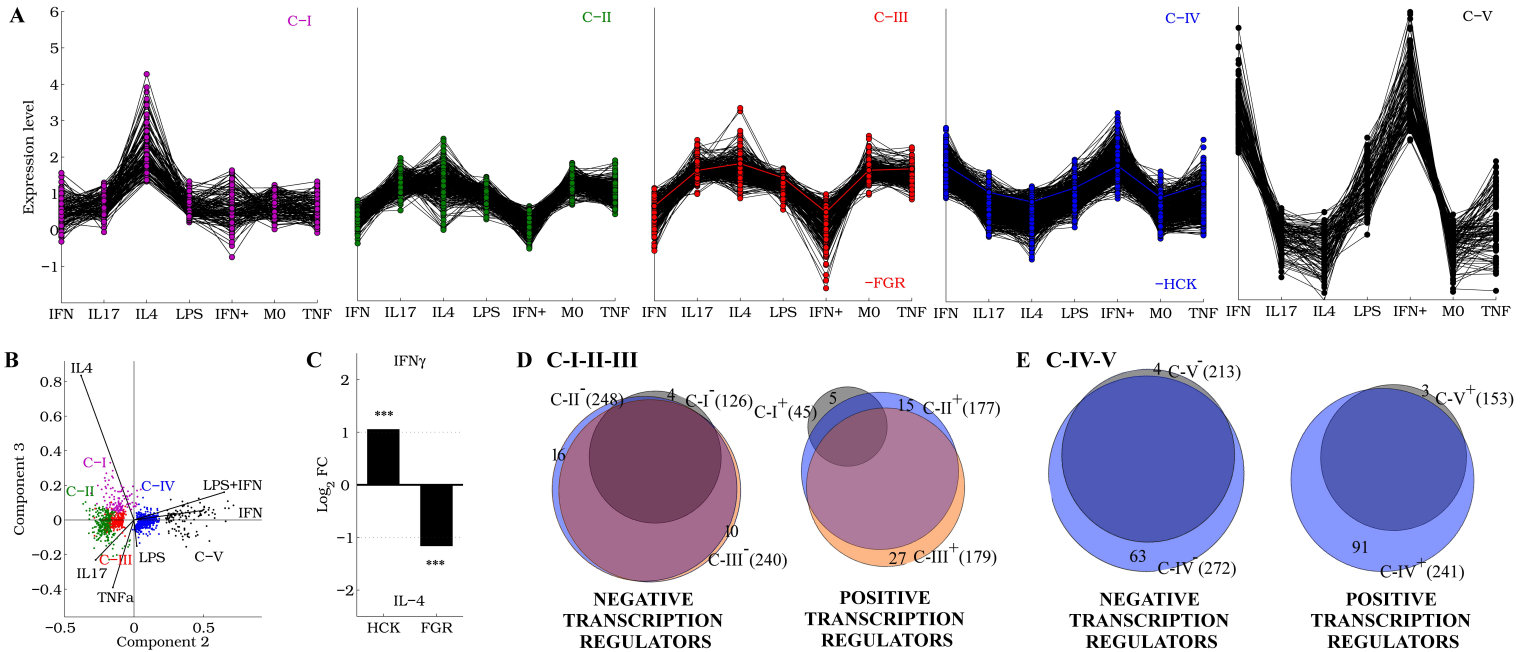

Figure. 2.9. *Transcriptome analysis of gene expression in human macrophages. A. K–means clustering of human genes modulated upon stimulation with IFNγ, IL–17, IL–4, LPS, IFNγ + LPS (denoted as IFN+) or TNFα generates five clusters (C-I to C-V). FGR and HCK belong to C-III and C-IV respectively (A). B. PCA of K–means clustered genes. 99.3% of the variance of the system lies within the first three PC (PC1:1.3, PC2:84.8 and PC3:13.2%). Two dimensional PC2 vs PC3 biplot projection of gene scores and component coefficients for each treatment. Note the divergent positioning of C-III (red) and C-IV (blue) along the PC2 axis. The direction and length of the vectors indicate how each treatment contributes to the components. C. HCK and FGR display opposite expression patterns in response to IFNγ and IL–4. D-E. Transcription factor analysis permitted the identification of positive and negative regulators of gene expression corresponding to CI to CIV. Euler diagrams indicate that positive regulators of gene expression were shared between clusters I-III (D) and clusters IV-V (E).*

REGULATOR	EXPRESSION PROFILE	REGULATED GENES(%) C-I	C-II	C-III
HIF2A/EPAS1	C-III	27	36	39
IRF4	C-I	9		
KLF2	C-I	18	26	31
KLF4	C-II	17	40	48
MAF	C-II	34	19	15
MYC	C-II	21	16	21
PPARG	C-III	40	48	59
SOCS1	C-III			
STAT3	C-III	27	60	73
STAT6	C-I	20	17	16

Figure. 2.10. *Transcription factors linked to tissue repair and resolution of inflammation, that control the expression of genes upregulated upon IL–4 stimulation. Top panel: Percentage of regulated genes per cluster($*P \prec 1E-5$). Bottom panel: bar graph view of genes regulated in cluster C-III. Vertical bars correspond to ranked positions of genes regulated, ordered by P value. The position is given by the red–blue gradient at the bottom of the graph, that represents the ranking between the highest (farthest left (red) and right (blue)) and the lowest (middle, white) test statistic, for differential expression. Red and blue vertical bars represent respectively genes that are positively or negatively correlated to the expression of each transcription factor.*

Network expansion was then performed to include all genes that did not present differential expression upon stimulation with TNFα, IL–4, IL–17, LPS, IFNγ or LPS+IFNγ, but which interact with genes in clusters C-I, C-II, C-III, C-IV and C-V (obtained by K–means analysis of differentially expressed genes). Networks N-I, N-II, N-III, N-IV and N-V were respectively obtained. Curated interactions where obtained from InnateDB database [104].

As expected, and in agreement with the reduced adhesion to the endothelium and deficient migration observed in double deficient macrophages (Fig. 2.2 to 2.6), both, HCK and FGR had common interactors involved in actin polymerization and filament organization (GO:0008154, GO:0007015, Benjamini Hochberg corrected over–representation $Pval \prec 1E-05$), cell migration (GO:0030335, GO:0050900, corrected $Pval \prec 1E-05$), cell adhesion (GO:0045785, corrected $Pval \prec 1E-02$) and podosome organization (GO:0071801, corrected $Pval \prec 1E-02$). In addition, HCK, FGR and their first neighbor interactors were found to over–represent the chemokine signaling pathway (corrected $Pval \prec 1E-05$) with downstream targets involved both

REGULATOR	EXPRESSION PROFILE	REGULATED GENES(%) C-IV	C-V
FOSB	C-IV		
HIF1A	C-IV	33	32
IKBKG		12	
JUND		5	13
NFKB1	C-IV	23	24
NFKB2	C-IV	40	66
SOCS3	C-IV		
STAT1	C-V	17	15
STAT2	C-IV	32	46
STAT5A		9	

Figure. 2.11. *Transcription factors linked to proinflammatory macrophage differentiation that control the expression of genes upregulated upon IFNγ stimulation. Top panel: Percentage of regulated genes per cluster ($*P \prec 1E-5$). Bottom panel: bar graph view of genes regulated in cluster C-IV. Vertical bars correspond to ranked positions of the genes regulated, ordered by P value. The position is given by the red–blue gradient at the bottom of the graph, that represents the ranking between the highest (farthest left (red) and right (blue)) and the lowest (middle, white) test statistic, for differential expression. Red and blue vertical bars represent respectively genes that are positively or negatively correlated to the expression of each transcription factor.*

in immune cell function and cell migration (Appendix A. Fig A.9).

Interestingly, while FGR was only present in N-III (Fig. 2.12A), as expected, HCK was included in N-I, N-II, N-III and N-IV (Fig. 2.12B, see below for a discussion). Similarly, many gene products were shared by more than one network (Fig. 2.12A-C), which suggest that they form part of a core set of proteins active in both classic and alternative macrophage differentiation.

Hck and Fgr are expected to participate in different biological processes, due to their differences in structure, and different classification among Src kinase subfamilies [110]. Network expansion facilitated the identifications of molecular interactions and functions not shared by HCK and FGR. In fact, inside its network, FGR, but not HCK, displayed multiple interactions with proteins that induce anti–inflammatory and tissue repairing programs, including the PPARG co–activator NCOA6 [111] and PXR (NR1I2), an anti–inflammatory protein that blocks NFKB activation [112–114] (Fig. 2.13A-b). In addition, FGR activates STAT3 [115], which is crucial

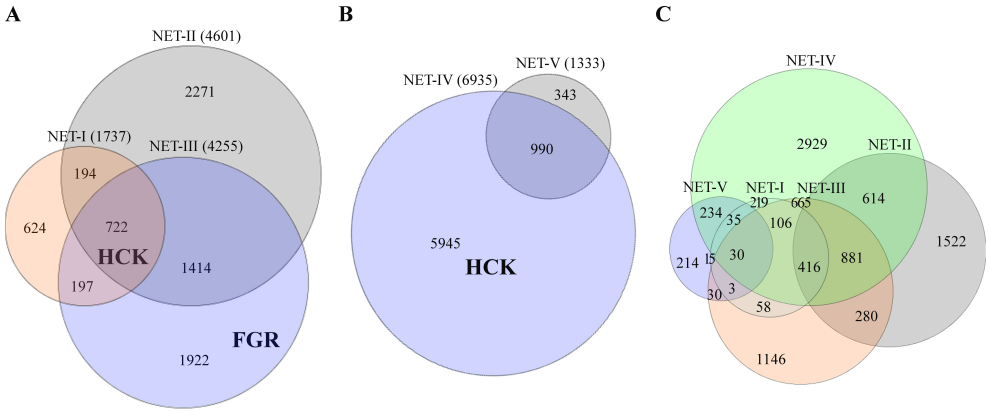

Figure. 2.12. *Euler diagram of gene networks expanded from Clusters I-V. A-C. Network expansion was performed using clusters of genes with similar expression profile in response to IFNγ, IL–17, IL–4, LPS, IFNγ + LPS or TNFα stimulation. Roman numbers for networks correspond to numbers of clusters in Fig 2.9. A. HCK and FGR participate in networks containing genes upregulated in response to IL–4 (C-I, C-II and C-III). B. HCK also participates in network N-V, containing genes upregulated in response to IFNγ. C. Expanded networks from clusters I-V contain genes particular for each network as well as genes that are shared. The overlap among networks indicates the presence of core genes that are used for both, anti–inflammatory (N-I, N-II and N-III) and pro–inflammatory (N-IV and N-V) processes.*

for anti–inflammatory and tissue repairing [116, 117] programing of macrophages (Fig. 2.13A-B). Furthermore, tyrosine phosphorylation of IKBKG by FGR (Fig. 2.13A), leads to suppression of NFKB activation [118], which positions FGR as an anti–inflammatory kinase(interaction of FGR but not HCK with NCOA6, NR1I2 and IKBKB respectively in [119–121]).

HCK on the other hand, mediates the activation of macrophages in response to LPS [122, 123] and IFNγ [124, 125] and was found to interact inside its network with proteins that promote inflammation, including (i) NCL which regulates the polarization of macrophages in response to LPS stimulation [126]; (ii) CREBBP, which cooperate with NFKB and STAT1 to mediate inflammatory gene expression upon IFNγ stimulation [127] and (iii) BTK a negative regulator of alternative activation in macrophages [128, 129] (interactions of HCK, not FGR, with NCL, CREBBP and BTK respectively in [130–132]).

In addition, tyrosine phosphorylation of p73 (TP73) by Hck represses its transcriptional activity [133], which is required for alternative activation of macrophages and macrophage induced resolution of inflammation [134]; arguing for a proinflammatory role of HCK in macrophage function.

It is therefore likely that besides their overlapping role in macrophage chemotaxis, Hck and Fgr have divergent roles to promote pro–inflammatory and wound healing processes, respectively. However, HCK was included in Networks N-I, N-II and N-III, obtained upon expansion of clusters C-I, C-II and C-III, respectively (Fig.

2.13B and 2.12). In these networks, HCK interacts with PI3K and its p85 regulatory subunit [130, 135], which are crucial for alternative activation of macrophages [55]. In addition, similar to FGR, HCK activates STAT3, to induce anti–inflammatory macrophage activation programs [82, 115] (Fig. 2.13B). Moreover, inhibition of Src tyrosine kinases has been demonstrated to block the activation of STAT6 [136], which is critical for alternative activation of macrophages [116, 117]. Similarly, Src tyrosine kinase dependent phosphorylation of SHIP triggers its polyubiquitination and degradation within the proteasome [137], which is required for alternative activation of macrophages by IL–4 [138].

It is therefore conceivable that HCK mediates both pro–inflammatory and tissue repairing programs in macrophages, in a context dependent fashion, implying that HCK deficiency might skew the balance of macrophage function towards both pro–and anti–inflammatory directions.

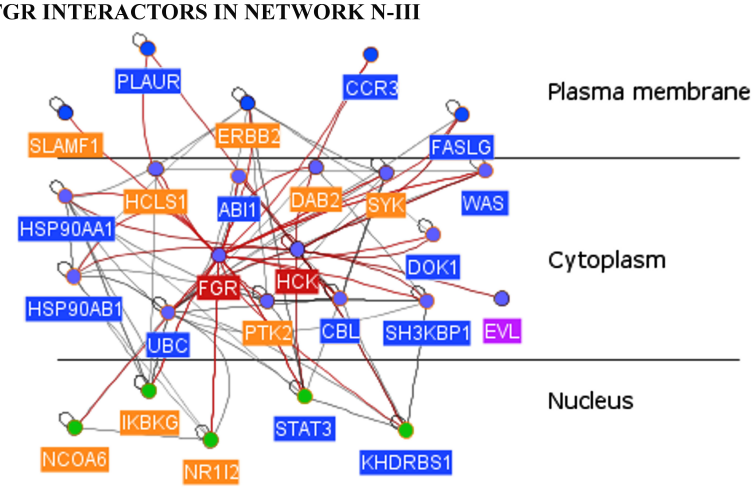

Figure. 2.13. *First neighbors of FGR and HCK, in Network N-III. Expansion of cluster C-III resulted in network N-III (see also Fig. 2.9). Shown here are HCK, FGR and their first interactor neighbors (orange labels for FGR interactors, blue, for HCK and FGR interactors, purple for HCK interactors). FGR, but not HCK, interacts with transcription factors that control the expression of anti–inflammatory genes (NCOA6 [111], NR1I2 [112–114]). Tyrosine phosphorylation of IKBKG by FGR, leads to suppression of NFKB activation [118]. STAT3 is activated by both, FGR (A) and HCK (B) [115]. Interactions of FGR, but not HCK, with NCOA6, NR1I2 and IKBKG in References: [119–121]. See text for further details.*

2.5 Discussion

This chapter presents conclusive evidence that demonstrates that Hck/Fgr–deficiency leads to reduced atherosclerotic lesion formation with concomitant reduction in macrophage accumulation and lesion stability due to impaired adhesion to the endothelium, altered mesenchymal migration and skewing of macrophage differentiation towards a

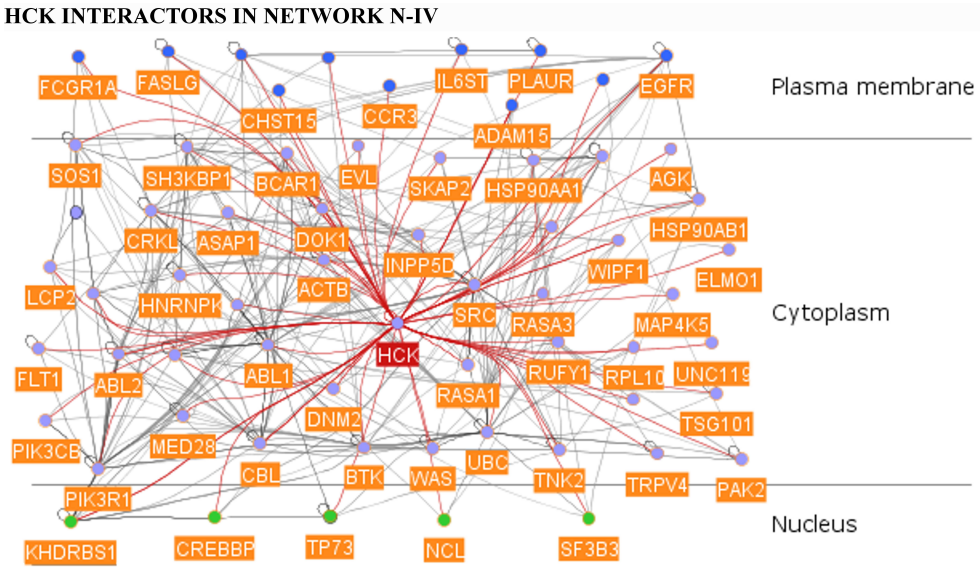

Figure. 2.14. *First neighbors of HCK, in network N-IV. Expansion of cluster C-IV resulted in network N-IV (see also Fig. 2.9). Shown here is HCK and its first interactor neighbors (orange labels). HCK, interacts with transcription factors that control the expression of pro–inflammatory genes (NCL [126], CREBBP [127], BTK [128, 129]). Tyrosine phosphorylation of TP73 by Hck represses its transcriptional activity [133], which is required for alternative activation of macrophages and macrophage induced resolution of inflammation [134]. Interactions of HCK but not FGR, with NCL, CREBBP, BTK and TP73 in References: [130–133]. See text for further details.*

pro–inflammatory phenotype.

As a first hallmark of Hck/Fgr–deficiency, atherosclerotic lesions displayed reduced amounts of macrophages despite higher availability of circulating Ly6c^{hi} monocytes, a subset known for its hypermigratory and inflammatory profile, and selective accumulation in atherosclerosis [57, 58].

Intravital microscopy of circulatory leukocytes, including monocytes and granulocytes; and chlodronate liposome labeling of Ly6c^{hi} demonstrated reduced myelocyte adhesion to the endothelium and extravasation into atherosclerotic lesions, in Hck/Fgr dKO chimeras. In addition, Hck/Fgr–deficient macrophages displayed impaired morphological polarization, deficient adhesion to the endothelium and disrupted two and three dimensional migration. Furthermore, dKO macrophages were unable to form filopodia and lamellipodia, which is critical for those cells to adhere and establish leading and trailing poles that direct their mobilization towards higher concentrations of chemoattractants [139]. Taken together, these results imply that Hck/Fgr–deficiency caused reduced adhesion on the endothelium and therefore reduced extravasation of circulating monocytes and accumulation of macrophages in atherosclerotic lesions.

The three–dimensional mesenchymal migration of macrophages depends on the formation of podosome rosettes, which release proteolytic enzymes to perform peri-

cellular degradation of the extracellular matrix [90]. *In-vitro*, dKO macrophages had impaired localized degradation of the extracellular matrix by disrupted formation of podosome rosettes, and mesenchymal migration. Considering the transformation of monocytes from amoeboid to mesenchymal migrating cells upon extravasation into peripheral tissues and differentiation into macrophages [140] this result indicates that Hck/Fgr–deficiency might have caused reduced macrophage mesenchymal migration across lesional fibrous caps, contributing this way to the reduced accumulation of macrophages observed in lesions of dKO chimeras.

A second striking hallmark of Hck/Fgr–deficiency was the high susceptibility to apoptosis induction that dKO macrophages displayed, and the expansion of necrotic cores observed in Hck/Fgr deficient, atherosclerotic mice. This, together with the inability of dKO macrophages to migrate suggest that intra–lesion phagocytes might have been unable to migrate towards apoptotic cell "eat me signals", leading to poor efferocytosis of death cells with subsequent expansion of necrotic cores.

Reduced fibrosis, VSMC accumulation and collagen deposition were also observed in atherosclerotic lesions of atherosclerotic mice recipients of dKO bone marrow cells. One likely explanation for this phenotype, is that reduced adhesion and homing of circulatory monocytes into atherosclerotic lesions might have caused reduced accumulation of fibrocytes. In fact, Lessened fibrocyte contents correlate with atherosclerotic lesion instability and reduced deposition of collagen and secretion of TGFβ [141, 142]. In addition, blood monocytes are known to differentiate into fibrocytes [143] that express Hck and Fgr [144] and accumulate in atherosclerotic fibrous caps [142], suggesting that Hck–Fgr deficiency would not also lead to reduced macrophage accumulation but also reduced numbers of lesion fibrocytes; a point that could be addressed by staining atherosclerotic lesions from Hck–Fgr deficient chimeras for markers that discriminate between monocytes, macrophages, fibrocytes, fibroblast and SMCs [144].

It is also likely that Hck and Fgr have a role in macrophage tissue repairing functions. In agreement with this notion, we demonstrated that Hck/Fgr–deficient macrophages inhibited VSMC extracellular matrix collagen and non–collagenous protein deposition. Similarly, ear excision wounds treated with Src tyrosine kinase inhibitors display reduced accumulation of collagen and wound healing [145]. Furthermore, Hck/Fgr–deficient chimeras displayed Ly6c^{hi} blood monocytosis, which correlates with higher Ly6c^{hi} monocyte infiltration into atherosclerotic lesions [57, 58], lesion vulnerability [59–61] and reduced accumulation of anti–inflammatory and tissue repairing macrophages [59, 61, 146].

Transcriptome and network analysis of microarray datasets indicated the involvement of HCK and FGR in human atherosclerosis (Appendix A. Fig. A.10) and gene networks that regulate inflammation and control the induction of tissue repair by macrophages. In agreement with these results, FGR has been reported to block the activation of NFKB [118] and activate STAT3 [115], which induces the expression of wound healing genes, including TFG-b and IL-10 [117, 147]. Fgr deficiency therefore, would be expected cause inflammation and extracellular matrix degradation.

Hck on the other hand, participates in divergent gene networks that drive macrophage pro–inflammatory and extracellular matrix degrading or anti–inflammatory and wound–healing functions, depending on the molecular network it is embedded in. This indicates that HCK is unlikely to be crucial for macrophage phenotypic polar-

ization, and implicates that the effect of Hck deficiency would be context dependent.

Taken as a whole, the results obtained by computational analysis indicate that Hck and Fgr double deficient macrophages would be expected be pro–atherogenic and induce reduced deposition of collagen, as observed in the experiments here presented. This sets the basis for further experimentation, to corroborate the dual and context dependent role of Hck and the function of FGR as anti–inflammatory kinase that positively regulates wound healing and tissue repair.

The prominent involvement of Hck/Fgr in extravasation and alternative activation of macrophages, shifts the paradigm of macrophage accumulation as prime responsible factor of lesion vulnerability towards the notion of intra–lesion macrophage phenotype as crucial determinant of plaque stability. The role of Hck and Fgr in chemotaxis and that of Fgr in wound healing and tissue repair, raises a note of caution against the use of Src kinase inhibitors for the treatment of atherosclerosis, where reduced macrophage accumulation with simultaneous increased tissue repair and deposition of collagen are desired to attain a stable plaque profile. However, the novel application of Src Kinase inhibitors as anti–fibrotic therapy in systemic sclerosis [148, 149] and the results here described, support their potential to treat the fibroplastic vasculopathy of restenosis and disorders where simultaneous reduction of extracellular matrix deposition and macrophage accumulation are desired (for a review see [150, 151]).